AIAA JOURNAL
Vol. 40, No. 1, January 2002

Design Optimization of Springback in a Deepdrawing Process

Kyung K. Choi* and Nam H. Kim†
University of Iowa, Iowa City, Iowa 52242

The design optimization of springback in a deepdrawing process is proposed to control the final shape of the workpiece. The manufacturing process design problem is formulated to minimize the difference between the shape of the desired workpiece geometry and the final analysis result after elastic springback. The rigid die shape and the workpiece thickness are treated as design variables. A nonlinear structural problem that includes finite deformation elastoplasticity with frictional contact is solved using a mesh-free method in which the structural domain is discretized by a set of particles. Continuum-based design sensitivity analysis is carried out to obtain gradient information for the optimization efficiently. The accuracy of the sensitivity result is compared with the finite difference result with excellent agreement. The optimum deepdrawing process significantly improves the quality of the final product.

I. Introduction

DESPITE significant simulation and design capability developments in modern technology, gaps still remain between the simulation-based design and the manufacturing process itself. One major reason for these gaps is the lack of efficient and accurate numerical methods in the design process. First, accurate numerical methods have to be used to simulate manufacturing processes, and these methods must take into account large deformations, complicated constitutive relations, and a sliding contact between workpiece and die. Second, efficient numerical methods have to be used to make the deepdrawing optimization process practical. It is the purpose of this paper to demonstrate that these two obstacles can be resolved by using accurate numerical methods and an efficient design sensitivity analysis (DSA).

The deepdrawing process involves a large degree of plastic deformation and rigid-body rotations, as well as a complicated contact between workpiece and die. Many simplified approaches have been proposed in simulation and design of the metal forming process. One major trend is to ignore the elastic deformation of the structure compared to the plastic part. Antunez and Kleiber,[1] Maniatty and Chen,[2] Zhao et al.,[3] Chung and Hwang,[4] and Balagangadhar and Tortorelli[5] used a rigid-plasticity formula to solve metal forming design problems. This approach is useful for problems of the bulk metal forging type. As shown in Sec. IV, however, the elastic springback at the end of a deepdrawing process plays an important role in determining the quality of the final product. Thus, in practice the constitutive relation that considers the elastic and plastic parts together has to be used. Lagrangian approaches of DSA in large deformation elastoplasticity were proposed by Badrinarayanan and Zabaras[6] and Wiechmann and Barthold.[7] However, they did not bring design capability of minimizing elastic springback. Guo et al.[8] proposed an inverse approach to optimize the sheet metal forming parts. However, they used a path-independent material model, which is only valid for the loading process. Because material is path independent, they developed an adjoint variable method for design sensitivity analysis, which is not applicable for the path-dependent material. Karafillis and Boyce[9] proposed an inverse springback calculation method to obtain the desired workpiece geometry after springback. They determined the shape of the tool based on the force that is required to springforward the workpiece. In the case of the vertical deepdrawing, however, the springforward method would not work because the vertical part of the punch cannot exceed more than 90 deg.

In this paper, the design optimization of a deepdrawing process is proposed to control the final shape of the workpiece after elastic springback. The manufacturing process design problem is formulated to minimize the difference between the shape of the desired workpiece geometry and analysis result after elastic springback. The amount of plastic strain and the reduction of workpiece thickness are design constraints that prevent material separation and distortion. The design parameters can be chosen from the thickness of the workpiece, the geometry of the die and punch, the frictional coefficient between contact surfaces, and the binder force, all of which can control the output quality of the manufacturing process. Accurate sensitivity information of the cost and constraint functions with respect to design parameters plays a critical role in effective design optimization. An important feature of this paper is to develop a method for calculating the design sensitivity information accurately and efficiently when the workpiece experiences finite elastoplastic deformation with complicated frictional contact constraints.

Two theories of continuum-based shape design sensitivity formulations previously developed by Kim et al. will be used: finite deformation elastoplasticity[10] and frictional contact.[11] For response analysis, the multiplicative decomposition of the deformation gradient into elastic and plastic parts is used for the hyperelastic-based plasticity constitutive model with respect to the intermediate configuration. The classical return-mapping algorithm of the small deformation plasticity theory is preserved by using the principal space of the Kirchhoff stress and logarithmic strain tensors. In addition, the tangent operator has the same form as the algorithmic tangent operator of the infinitesimal theory. For shape design sensitivity, the shape variation is taken at the undeformed geometry of the workpiece, die, and punch. The path dependency of the sensitivity formulation comes from the evolution of the intermediate configuration and the internal plasticity variables, as well as the frictional effect in contact constraint. The numerical example shows the accuracy and efficiency of design sensitivity computation compared to those from the finite difference method.

When a structure experiences a finite deformation, the conventional finite element method may encounter difficulties in response analysis as a result of mesh distortion. Mesh regeneration may not be an effective method for resolving this difficulty. In addition, for shape design problems, mesh distortion is of major concern due to large shape design perturbations. An effective numerical method that can handle mesh distortion is highly desirable for both nonlinear analysis and shape optimization. The mesh-free method[12,13] is an ideal choice because, unlike the conventional finite element

Presented as Paper 2000-4747 at the AIAA/USAF/NASA/ISSMO 8th Symposium on Multidisciplinary Analysis and Optimization, Long Beach, CA, 6–8 September 2000; received 25 September 2000; revision received 30 June 2001; accepted for publication 4 July 2001.

*Professor and Director, Center for Computer-Aided Design and Department of Mechanical Engineering, College of Engineering; kkchoi@ccad.uiowa.edu. Associate Fellow AIAA.

†Postdoctoral Associate, Center for Computer-Aided Design and Department of Mechanical Engineering, College of Engineering; nkim@ccad.uiowa.edu. Member AIAA.

method, the solution is much less sensitive to mesh distortion. In the mesh-free method, the structural domain is discretized with a finite number of particles whereas, in the finite element method, it is discretized with nodes and elements. The shape function at a point is constructed based on a set of scatter particles surrounding that point. To construct shape function, modified kernel functions are used to enforce the reproducing conditions. As a result, the kernel approximation of displacements exactly reproduces a certain class of polynomial. In this paper, the mesh-free method is used in the nonlinear response analysis and, thus, the design sensitivity analysis of manufacturing process optimization.

II. Deepdrawing Analysis

A. Elastoplasticity in Finite Deformation

The classical theory of elastoplasticity assumes the additive decomposition of the elastic and plastic strains. Small deformation and small rigid-body rotation are assumptions in this theory. Even if much research on the objective rate were carried out in the large deformation problem, the question concerning numerical integration methods that satisfy all of the physical requirements[14] for the objective rate still remains. The difficulty in obtaining an exact tangent stiffness operator causes an error in DSA, and this error is accumulated as the simulation progresses. In this paper, kinematics proposed by Lee[15] are used where the deformation gradient $\boldsymbol{F}(\boldsymbol{X}) = \partial \boldsymbol{x}/\partial \boldsymbol{X}$ is decomposed multiplicatively into elastic and plastic parts, namely,

$$\boldsymbol{F}(\boldsymbol{X}) = \boldsymbol{F}^e(\boldsymbol{X})\boldsymbol{F}^p(\boldsymbol{X}) \tag{1}$$

where $\boldsymbol{F}^p(\boldsymbol{X})$ denotes the deformation through the intermediate configuration, which is related to the internal variables, and $\boldsymbol{F}^{e-1}(\boldsymbol{X})$ defines the local, stress-free, unloaded process. In Eq. (1), $\boldsymbol{X}$ represents the material point at the undeformed domain Ω_X and $\boldsymbol{x}$ denotes the material point at the current domain Ω_x. The stress–strain relation is given as a hyperelasticity between the intermediate and the current configurations. A computational framework of this theory is proposed by Simo[16] that preserves the conventional return-mapping algorithm in the principal stress space.

By using the principle of virtual work, the structural problem is formulated in a weak form to find the displacement z that satisfies

$$a_\Omega(z, \bar{z}) = \ell_\Omega(\bar{z}), \qquad \forall \bar{z} \in Z \tag{2}$$

where Z is the space of kinematically admissible displacements that satisfy the homogeneous, essential boundary conditions. In this paper, the superposed bar is used to denote a variation, such that $\bar{z}$ represents the displacement variation or the virtual displacement. Equation (2) contains finite deformation, including elastoplasticity and rigid-body rotation. In Eq. (2), $a_\Omega(z, \bar{z})$ and $\ell_\Omega(\bar{z})$ are the structural energy and load forms, respectively, defined as

$$a_\Omega(z, \bar{z}) = \iint_{\Omega_X} \tau_{ij}\varepsilon_{ij}(\bar{z})\, \mathrm{d}\Omega \tag{3}$$

$$\ell_\Omega(\bar{z}) = \iint_{\Omega_X} \bar{z}^T \boldsymbol{f}^b\, \mathrm{d}\Omega + \int_{\Gamma_X^h} \bar{z}^T \boldsymbol{f}^h\, \mathrm{d}\Gamma \tag{4}$$

where τ_{ij} is the Kirchhoff stress tensor, $\varepsilon_{ij} = \frac{1}{2}(z_{i,j} + z_{j,i})$ the engineering strain at the current configuration, $\boldsymbol{f}^b$ the body force per unit volume, and $\boldsymbol{f}^h$ the surface traction on the traction boundary Γ_X^h. Only a conservative load is considered in Eq. (4). The computation of τ_{ij} in Eq. (3) involves hyperelasticity using $\boldsymbol{F}^e$ in Eq. (1) and the return-mapping algorithm in the principal stress space. The dependence of $a_\Omega(z, \bar{z})$ on z is nonlinear due to the elastoplastic constitutive relation and due to nonlinear kinematics.

The nonlinear variational Eq. (2) can be solved for displacement z iteratively using the Newton–Raphson method, which requires the linearization of the structural energy form in Eq. (3) with respect to the displacement increment Δz, as[11]

$$a_\Omega^*(z; \Delta z, \bar{z}) = \iint_{\Omega_X} \varepsilon_{ij}(\bar{z}) C_{ijkl}^{\mathrm{alg}} \varepsilon_{kl}(\Delta z)\, \mathrm{d}\Omega + \iint_{\Omega_X} \tau_{ij}\eta_{ij}(\Delta z, \bar{z})\, \mathrm{d}\Omega \tag{5}$$

where C_{ijkl}^{alg} is the fourth-order consistent tangent stiffness tensor[16] and $\tau_{ij}\eta_{ij}$ is the initial stiffness term. Note that $a_\Omega^*(z; \Delta z, \bar{z})$ is linear with respect to its arguments. The computational frame-work of nonlinear analysis follows the incremental procedure. For example, let the current time be t_n, and let the iteration counter be $k+1$; then the linearized incremental problem of Eq. (2) is

$$a_\Omega^*({}^n z^k; \Delta z^{k+1}, \bar{z}) = \ell_\Omega(\bar{z}) - a_\Omega({}^n z^k, \bar{z}), \qquad \forall \bar{z} \in Z \tag{6}$$

The linear variational Eq. (6) is solved until the right-hand side (residual force) vanishes, which means that the original nonlinear Eq. (2) is satisfied at t_n. After the solution is converged in Eq. (6), the plastic internal variables (back stress and effective plastic strain), as well as $\boldsymbol{F}^p$ in Eq. (1), are updated to the current configuration.

B. Frictional Contact

A contact analysis that includes interactions between the workpiece and punch/die is critical in simulating the deepdrawing process. Among the many contact formulations, the penalty regularization method is used in this paper, in which a small penetration is allowed between the workpiece and rigid surface. Let Γ_C be the region where the workpiece penetrates the rigid surface at the current configuration. Then this region is penalized in proportion to the amount of penetration g_n. The contact variational form is defined as

$$b_\Gamma(z, \bar{z}) = \omega_n \int_{\Gamma_C} g_n \bar{z}^T \boldsymbol{e}_n\, \mathrm{d}\Gamma + \begin{cases} \omega_t \displaystyle\int_{\Gamma_C}^{+} \nu g_t \bar{z}^T \boldsymbol{e}_t\, \mathrm{d}\Gamma & \text{if} \quad |\omega_t g_t| \le |\mu \omega_n g_n| \\ -\mu\omega_n \operatorname{sgn}(g_t) \displaystyle\int_{\Gamma_C} \nu g_n \bar{z}^T \boldsymbol{e}_t\, \mathrm{d}\Gamma & \text{otherwise} \end{cases} \tag{7}$$

where ω_n and ω_t are the normal and tangential penalty parameters, $\boldsymbol{e}_n$ and $\boldsymbol{e}_t$ are the unit normal and tangent vectors at the contact point, g_n and g_t are the normal gap and tangential slip, and μ is the frictional coefficient in Coulomb law. Note that Eq. (7) includes two conditions: the stick condition ($|\omega_t g_t| \le |\mu\omega_n g_n|$) in which a microscopic-elastic motion exists between contact surfaces and the slip condition in which a macroscopic-permanent motion exists. Because of the stick condition, this is a regularized Coulomb friction model as shown in Fig. 1.

The contact variational form in Eq. (7) is nonlinear in displacement because variables g_n, g_t, $\boldsymbol{e}_n$, and $\boldsymbol{e}_t$ implicitly depend on the displacement and because the contact region itself is not known a priori. The same method used to linearize the structural energy form in Eq. (5) can also be used to linearize the contact variational form in Eq. (7). The linearized variational equation, including the frictional contact constraint, is

$$a_\Omega^*({}^n z^k; \Delta z^{k+1}, \bar{z}) + b_\Gamma^*({}^n z^k; \Delta z^{k+1}, \bar{z}) = \ell_\Omega(\bar{z}) - a_\Omega({}^n z^k, \bar{z}) - b_\Gamma({}^n z^k, \bar{z}), \qquad \forall \bar{z} \in Z \tag{8}$$

where $b_\Gamma^*(z; \Delta z, \bar{z})$ is the linearized contact variational form obtained by linearization of Eq. (7). Detailed expression of $b_\Gamma^*(z; \Delta z, \bar{z})$ can be found in Ref. 11, in which two separate expressions of $b_\Gamma^*(z; \Delta z, \bar{z})$ are derived for stick and slip conditions, respectively.

C. Mesh-Free Discretization and Nodal Integration

The continuum-based formulation of the structural problem in Eq. (8) has to be numerically approximated. As a result, the accuracy and stability of the solution critically depend on the numerical method employed. A mesh-free method,[12] in which the structural

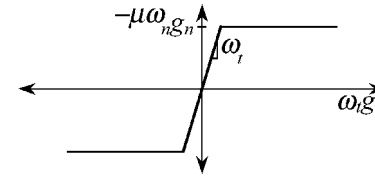

Fig. 1 Regularized Coulomb friction model.

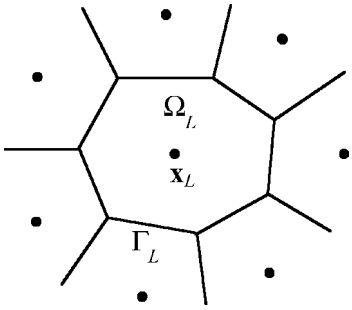

Fig. 2 Voronoi diagram of the scattered particle set.

domain is discretized by a set of particle points, is used in this paper. In the mesh-free method, each particle point has a finite support size that defines the domain of influence. Among the total NP number of particles in the domain, let IP be the number of particles whose support size covers the point $\boldsymbol{X}$. Then, the state variable z is approximated as

$$z(\boldsymbol{X}) = \sum_{I=1}^{IP} \Psi_I(\boldsymbol{X}) d_I \tag{9}$$

where $\Psi_I(\boldsymbol{X})$ is the mesh-free shape function and d_I is the coefficient of approximation. $\Psi_I(\boldsymbol{X})$ is constructed to satisfy the completeness condition that Eq. (9) exactly represents a certain order of polynomials. In the mesh-free method, the smoothness of approximation is easily controlled by the order of kernel function (p adaptivity). Because particles are not connected to the finite element, the insertion of additional particles to the structure is easily accomplished (h adaptivity). Unlike finite element approximation, however, because $\Psi_I(\boldsymbol{X})$ in Eq. (9) is a function of global material point $\boldsymbol{X}$ and d_I is not the value of the displacement at node I in general, more computational efforts are required than in finite element analysis.

The numerical integration of Eq. (8) is carried out using a nodal integration method,[17] in which the instability problem that exists in early development is resolved using a strain-smoothening algorithm. Figure 2 shows a typical example of domain partitioning using the Voronoi diagram. The nodal volume (area) is used as a weight for the domain integration.

With the approximation in Eq. (9) and numerical integration, the discretized variational equation is obtained for the given Sobolev space $H^1(\Omega)$, as

$$\bar{\boldsymbol{d}}^T \boldsymbol{K} \boldsymbol{d} = \bar{\boldsymbol{d}}^T \boldsymbol{F}, \qquad \forall \bar{\boldsymbol{d}} \in H^1 \tag{10}$$

where $\boldsymbol{K}$ is the global tangent stiffness matrix and $\boldsymbol{F}$ is residual force vector. Because the variation of the generalized displacement $\boldsymbol{d} = [\boldsymbol{d}_1, \boldsymbol{d}_2, \ldots, \boldsymbol{d}_{\mathrm{NP}}]^T$ is not nodal displacement, the imposition of the essential boundary condition is nontrivial in Eq. (10). Among the many proposed algorithms, the mixed boundary transformation method[18] is used in this paper to improve the efficiency of the analysis, while maintaining the accuracy of the solution.

III. DSA

The DSA is used to obtain the derivative of performance measures with respect to design variables. Despite some attractive features of the adjoint variable method in linear problems,[19] it is very complicated and expensive to apply to nonlinear path-dependent problems. Only the direct differentiation method, which is used in this paper, is applicable to general nonlinear path-dependent problems.

The shape design is usually more effective than the sizing design in improving performance measures. Because the design is the structural domain, each material point moves in the design direction. The material derivative concept in continuum mechanics is used to represent variation in a shape.

A. Shape Design of Elastoplasticity

The classical theory of the shape DSA in a linear problem is formally applied to nonlinear problems, even though no mathematical proofs of the existence and uniqueness of design sensitivity are available. Because the configuration of the nonlinear problem changes as simulation progresses, it is necessary to transform the current configuration to the initial domain, where a design velocity is defined, before the design derivative is taken.

The material derivative of the displacement vector ($\dot{z}$) can be expressed as a sum of the partial derivative and convective term as

$$\dot{z} = z' + \nabla z \boldsymbol{V} \tag{11}$$

where $\nabla = \partial/\partial \boldsymbol{X}$ is the gradient operator at the initial configuration and $\boldsymbol{V}$ is the design velocity vector that represents the direction of the design change. The direct differentiation method calculates $\dot{z}$ in Eq. (11) for the given design velocity vector $\boldsymbol{V}$ as follows. The material derivative of the nonlinear equation (2) at the perturbed design can be taken, using Eq. (11), to obtain

$$a^*_\Omega(z; \dot{z}, \bar{z}) = \ell'_V(\bar{z}) - a'_V(z, \bar{z}), \qquad \forall \bar{z} \in Z \tag{12}$$

where

$$a'_V(z, \bar{z}) = \int\!\!\int_{\Omega_X} \left(\bar{\varepsilon}_{ij} C^{\mathrm{alg}}_{ijkl} \varepsilon^V_{kl} + \tau_{ij} \eta^V_{ij}(z, \bar{z}) + \tau_{ij} \bar{\varepsilon}_{ij} \operatorname{div} \boldsymbol{V} \right) \mathrm{d}\Omega$$

$$+ \int\!\!\int_{\Omega_X} \left(\bar{\varepsilon}_{ij} C^{\mathrm{alg}}_{ijkl} \varepsilon^p_{kl} + \tau_{ij} \eta^p_{ij}(z, \bar{z}) + \bar{\varepsilon}_{ij} \tau^{\mathrm{fic}}_{ij} \right) \mathrm{d}\Omega \tag{13}$$

$$\ell'_V(\bar{z}) = \int\!\!\int_{\Omega_X} [\bar{z}^T (\nabla \boldsymbol{f}^b \boldsymbol{V}) + \bar{z}^T \boldsymbol{f}^b \operatorname{div} \boldsymbol{V}] \, \mathrm{d}\Omega$$

$$+ \int_{\Gamma^h_X} \left[\bar{z}^T (\nabla \boldsymbol{f}^h \boldsymbol{V}) + \kappa \bar{z}^T \boldsymbol{f}^h V_n \right] \mathrm{d}\Gamma \tag{14}$$

are the structural and external load fictitious forms, respectively. In Eq. (14), the applied load is assumed to be independent of any structural deformations, that is, conservative load, with κ as the curvature of the traction boundary whose normal component of design velocity is V_n. The structural fictitious form in Eq. (13) contains explicitly dependent terms on design in the first integral and path-dependent terms in the second integral. The path-dependent terms include material derivatives of the internal plastic variables and intermediate configuration as defined in Eq. (1). For detailed derivations of Eqs. (13) and (14), refer to Ref. 10.

Note that Eq. (12) has the same left-hand side as linearized structural Eq. (6) if $\dot{z}$ is replaced by Δz. Thus, the same tangent stiffness matrix $\boldsymbol{K}$, which is already factorized from analysis, can be used for very efficient sensitivity computation. After solving the sensitivity Eq. (11) for $\dot{z}$ up to the final configuration, sensitivity of the performance measures can be calculated using the chain rule of differentiation.

B. Die Shape Design

The purpose of the die shape DSA is to investigate the change of the performance measure when the shape of the punch/die changes. A die shape design optimization is very important in the manufacturing process because a simple geometry of the workpiece is normally used to obtain a complicated final product using the punch/die shape. The shape of the die can be changed in a similar procedure to the structural shape design perturbation by defining a design velocity field on the punch/die geometry. The shape perturbation of the die affects the performance of the workpiece through the contact variational form in Eq. (7). When the material derivative of Eq. (7) is taken and it is combined with the structural sensitivity Eq. (12), a design sensitivity equation is obtained as

$$a^*_\Omega(z; \dot{z}, \bar{z}) + b^*_\Gamma(z; \dot{z}, \bar{z}) = \ell'_V(\bar{z}) - a'_V(z, \bar{z}) - b'_V(z, \bar{z}) \qquad \forall \bar{z} \in Z \tag{15}$$

where the contact contribution of the fictitious load is denoted by $b'_V(z, \bar{z})$. It is shown by Kim et al.[11] that the contact fictitious load $b'_V(z, \bar{z})$ is path independent for the frictionless contact problem and path dependent for the fictional contact problem. Note that the design sensitivity equation (15) is linear, although the structural analysis is nonlinear.

C. Mesh-Free Implementation

A major difference between finite element and mesh-free methods is that the shape function of the mesh-free approach depends on

the coordinates of material points. Thus, for the material derivative of z,

$$\dot{z}(X) = \sum_{I=1}^{IP} \Psi_I(X)\dot{d}_I + \sum_{I=1}^{IP} \dot{\Psi}_I(X)d_I \tag{16}$$

The second term on the right-hand side of Eq. (16) is the contribution of the mesh-free shape function on the shape design and can be obtained explicitly in terms of the design velocity vector V. Thus, the contribution from this second term needs to be accounted for for the structural fictitious form in Eq. (13).

After the same assembly procedure as for the structural analysis is followed, the discretized design sensitivity equation can be obtained as

$$\bar{d}^T K\dot{d} = \bar{d}^T(F_\ell - F_a - F_b), \qquad \forall \bar{d} \in H^1 \tag{17}$$

where F_ℓ is the contribution from the applied load, F_a is the contribution from the structural energy, and F_b is the contribution from the contact constraints. Equation (17) is solved for $\dot{d}$, the material derivative of the generalized displacement. The sensitivity of the physical displacement can be obtained from Eq. (16). After solving Eq. (17) at the current time step, path-dependent variables have to be updated for the sensitivity computation at the next time step. The internal variables include all plastic evolution variables (effective plastic strain and back stress), the intermediate configuration that is defined by F^p in Eq. (1), and the displacement at the contact point caused by friction. When the design sensitivity equation is solved up to the final configuration time, the sensitivity of the performance measure can be obtained using the chain rule of differentiation. A possible list of performance measures would include workpiece area, displacement, stress, back stress, effective plastic strain, contact force, drawing force through punch, and the shape difference between the desired and final geometry after springback.

IV. Design Optimization

Design optimization of the deepdrawing process includes the parameterization of design, nonlinear mesh-free analysis, shape DSA, and optimization algorithm. MSC/PATRAN,[20] which uses a parametric representation, is used as the geometric modeling tool. An efficient method of design velocity computation in the parametric space was proposed by Choi and Chang.[21] Very accurate and efficient sensitivity results have been obtained to improve the convergence of the optimization iteration.

A. Design Parameterization

Figure 3 shows simulation setting and design parameterization of the deepdrawing process. Only half of the model is solved using symmetric conditions in the plane strain problem. The blank is modeled with 303 mesh-free particles. The von Mises yield criterion is used with an isotropic hardening model. A constant frictional coefficient is used in the modified Coulomb law. The draw die is fixed during the punch motion stage, and the blank holder exerts force to prevent any vertical movement of the blank. After simulating the maximum downstroke of punch (30 mm), the punch, die, and blank holder are removed to calculate springback.

The first two design parameters control the horizontal and vertical position of the punch. Horizontal movement is very important because it controls the gap between punch and draw die. The third and fourth parameters are round radii of the punch and draw die corners. A sharp corner may increase the plastic strain while reducing the amount of springback. The fifth parameter changes the thickness of the blank, which involves changes in the workpiece's shape. The sixth parameter controls the gap between the blank holder and die and allows the frictional force on the blank to be changed.

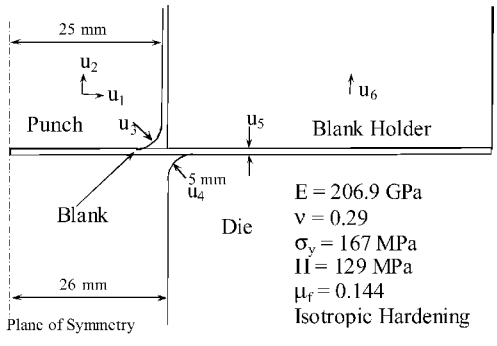

Fig. 3 Design parameterization of deepdrawing process.

B. Mesh-Free Nonlinear Analysis

Nonlinear mesh-free analysis is carried out to simulate spingback in the deepdrawing process. Rigid materials are assumed for the punch, drawing die, and blank holder. Thus, numerical integration is involved only for the workpiece material. A displacement-driven method is used so that the position of the punch is given at each time step. Converged configuration is found using the implicit Newton–Raphson method. For the stress computation, an elastic predictor, followed by a plastic return mapping, is used in the principal Kirchhoff stress. After finding a converged configuration, the factorized tangent stiffness matrix is stored to be used later for DSA purposes.

A slave–master concept is used for the contact problem to impose a penalty regularization. The rigid surfaces (punch, draw die, and blank holder) are modeled as piecewise linear master segments. With linear discretization, a very simple expression of $b_\Gamma(z, \bar{z})$ can be obtained because the normal and tangential vectors on the contact surface remain constant. However, the possibility exists of a convergence problem at the kinked corners of adjacent linear master segments. A line search algorithm is used when the convergence problem occurs. The contact search is carried out for particles on the domain boundary. If penetration into the rigid surface is detected, then a penalty is imposed using $b_\Gamma(z, \bar{z})$ in Eq. (7). Stick/slip conditions are determined by measuring the amount of motion relative to two adjacent configurations.

Figure 4 shows the deformation history of the workpiece along with its punch movement. Figure 5 shows the results of nonlinear analysis at maximum deformation and after springback. A significant amount of material sliding is observed between the workpiece and the draw die despite the considerable friction. The springback occurs when the punch, draw die, and blank holder are removed. Although the amount of elastic springback is relatively small at each part of the blank, the total displacement at the edge increases because of the rotational effect.

Figure 6 provides a contour plot of effective plastic strain at the moment of its final configuration. High plastic strain distribution is observed in the vertical section. A design constraint is imposed for the maximum allowable amount of plastic strain to prevent material failure due to excessive plastic deformation. In this paper the

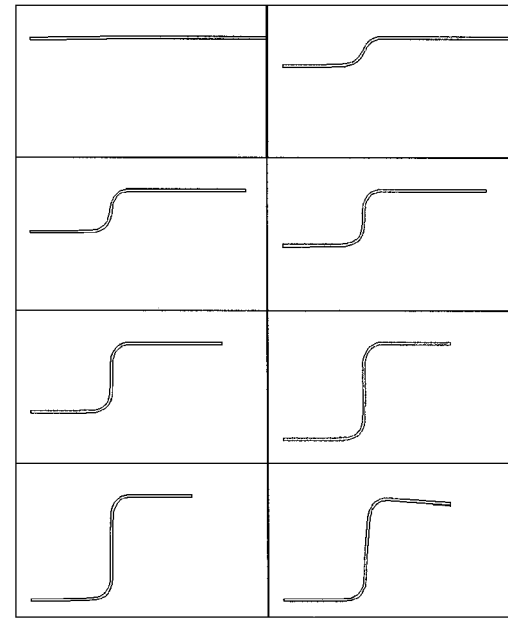

Fig. 4 Deformation history of the workpiece.

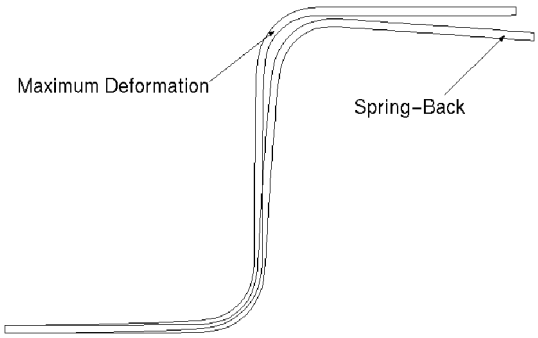

Fig. 5 Deepdrawing analysis with springback.

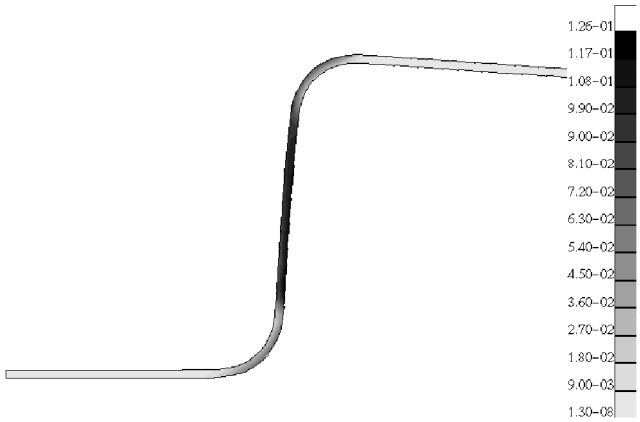

Fig. 6 Effective plastic strain distribution.

maximum allowable amount of effective plastic strain is assumed to be 0.2.

C. Sensitivity Analysis

Because there are six design parameters, design sensitivity Eq. (15) is solved six times, at each converged load step. Thus, an efficient method for solving the linear system of equations is very important for the computational cost. The performance measures are chosen for the effective plastic strain e^p and the shape difference G between the maximum deformation and after springback. Because the effective plastic strain is a path-dependent variable and its sensitivity is updated at each configuration, no additional computation is required to compute the sensitivity of e^p. The shape difference G is a function of the material points at the final configuration. Thus, the sensitivity of G can be calculated using $\dot{z}$ and the chain rule of differentiation as

$$\frac{\mathrm{d}}{\mathrm{d}\tau}[G(\boldsymbol{x})]|_{\tau=0} = \frac{\partial G^T}{\partial \boldsymbol{x}}(\boldsymbol{V}+\dot{z}) \tag{18}$$

The accuracy of DSA can be compared with the finite difference result by slightly perturbing the design and resolving the same structural problem. The finite difference method computes the sensitivity of the performance measure ψ by

$$\Delta\psi \approx \frac{\psi(\boldsymbol{x}+\Delta\tau\boldsymbol{V})-\psi(\boldsymbol{x})}{\Delta\tau} \tag{19}$$

for small $\Delta\tau$, which strongly depends on the accuracy of the structural analysis and machine operational error.

The continuum-based design sensitivity method proposed in this paper yields very accurate and efficient results. Table 1 compares the accuracy of the proposed sensitivity ψ' of various performance measures and $\Delta\psi$ with excellent agreements. A very small perturbation ($\Delta\tau = 10^{-6}$) is used for finite difference results.

In Table 1, the design sensitivity of performance G does not agree as much as other performance measures. The reason is that the magnitude of the performance change is large compared to the other performance measures. For example, the sensitivity of G is 10^3 times larger than the other performance measures for u_6. Thus, the finite difference method in Eq. (19) contains a large approximation error. This error will be reduced if perturbation size is decreased, although this may result in other performance measure inaccuracies due to numerical error. In short, it is very difficult to choose an appropriate perturbation size using the finite difference method.

The mesh-free analysis costs to solve the deepdrawing problem in Fig. 5 would be 8082 s on a Hewlett–Packard Exemplar workstation, whereas DSA would require 1843 s for six design parameters, which corresponds to a 3.8% analysis cost per design parameter. Such efficiency is expected because sensitivity analysis uses a decomposed

Table 1 Accuracy of sensitivity results

ψ	$\Delta\psi$	ψ'	$\Delta\psi/\psi' \times 100$
		u_1	
e^p_{41}	1.48092 $E-08$	1.48111 $E-08$	99.99
e^p_{45}	1.39025 $E-09$	1.38995 $E-09$	100.02
e^p_{55}	2.92573 $E-08$	2.92558 $E-08$	100.01
e^p_{142}	6.42704 $E-09$	6.42645 $E-09$	100.01
e^p_{147}	8.75082 $E-09$	8.75167 $E-09$	99.99
e^p_{152}	−4.88503 $E-08$	−4.88486 $E-08$	100.00
e^p_{157}	−2.08880 $E-08$	−2.08875 $E-08$	100.00
G	−4.31897 $E-05$	−4.37835 $E-05$	98.64
		u_2	
e^p_{41}	−7.51065 $E-10$	−8.28304 $E-10$	90.68
e^p_{45}	−8.63393 $E-09$	−8.77018 $E-09$	98.45
e^p_{55}	−3.46566 $E-08$	−3.32805 $E-08$	104.13
e^p_{142}	−1.02204 $E-08$	−1.02214 $E-08$	99.99
e^p_{147}	2.30561 $E-09$	2.27053 $E-09$	101.55
e^p_{152}	5.58534 $E-08$	5.58827 $E-08$	99.95
e^p_{157}	2.49171 $E-08$	2.41362 $E-08$	103.24
G	2.51654 $E-05$	2.57379 $E-05$	97.78
		u_3	
e^p_{41}	−1.81265 $E-09$	−1.81292 $E-09$	99.99
e^p_{45}	−8.32899 $E-10$	−8.33645 $E-10$	99.91
e^p_{55}	−1.60858 $E-08$	−1.60891 $E-08$	99.98
e^p_{142}	−4.17814 $E-09$	−4.17970 $E-09$	99.96
e^p_{147}	−8.43008 $E-10$	−8.43061 $E-10$	99.99
e^p_{152}	2.65440 $E-08$	2.65487 $E-08$	99.98
e^p_{157}	1.14224 $E-08$	1.14229 $E-08$	99.99
G	1.50596 $E-05$	1.55745 $E-05$	96.69
		u_4	
e^p_{41}	−1.64206 $E-08$	−1.64212 $E-08$	100.00
e^p_{45}	−1.78461 $E-08$	−1.78462 $E-08$	100.00
e^p_{55}	−2.06306 $E-08$	−2.06324 $E-08$	99.99
e^p_{142}	5.10648 $E-09$	5.10589 $E-09$	100.01
e^p_{147}	−9.75899 $E-09$	−9.75881 $E-09$	100.00
e^p_{152}	−1.46721 $E-08$	−1.46709 $E-08$	100.01
e^p_{157}	−1.65305 $E-08$	−1.65318 $E-08$	99.99
G	5.16216 $E-05$	5.47740 $E-05$	94.24
		u_5	
e^p_{41}	6.32293 $E-07$	6.33335 $E-07$	99.84
e^p_{45}	−3.42150 $E-07$	−3.41924 $E-07$	100.07
e^p_{55}	1.01051 $E-06$	1.01077 $E-06$	99.97
e^p_{142}	4.27720 $E-07$	4.28280 $E-07$	99.87
e^p_{147}	−6.64596 $E-07$	−6.64791 $E-07$	99.97
e^p_{152}	−2.43935 $E-06$	−2.43989 $E-06$	99.98
e^p_{157}	−1.54750 $E-06$	−1.54754 $E-06$	100.00
G	−8.01735 $E-04$	−8.51401 $E-04$	94.17
		u_6	
e^p_{41}	5.21628 $E-07$	5.22109 $E-07$	99.91
e^p_{45}	−2.04683 $E-07$	−2.05656 $E-07$	99.53
e^p_{55}	1.20942 $E-06$	1.20331 $E-06$	100.51
e^p_{142}	4.41449 $E-07$	4.42033 $E-07$	99.87
e^p_{147}	−5.38989 $E-07$	−5.39373 $E-07$	99.93
e^p_{152}	−2.39527 $E-06$	−2.39169 $E-06$	100.15
e^p_{157}	−1.42736 $E-06$	−1.42780 $E-06$	99.97
G	−1.19663 $E-03$	−1.25937 $E-03$	95.02

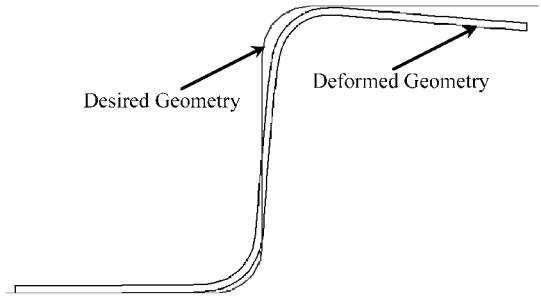

Fig. 7 Shape difference between deformed geometry and desired geometry.

tangent stiffness matrix, and no iteration is required for sensitivity computations.

D. Design Optimization

As mentioned before, the design optimization problem is formulated to minimize

$$G = \sum [P(\boldsymbol{x}_i) - \boldsymbol{x}_i]^2$$

subject to

$$e^p \le 0.2, \qquad t_i \ge 0.6, \qquad -0.1 \le u_1 \le 0.1$$
$$-0.01 \le u_2 \le 0.1, \qquad -1.1 \le u_3 \le 1.1, \qquad -1.1 \le u_4 \le 1.1$$
$$-0.01 \le u_5 \le 0.01, \qquad -0.02 \le u_6 \le 0.1 \qquad (20)$$

where $P(\boldsymbol{x})$ is the orthogonally projected position of the particle $\boldsymbol{x}$ on the desired final workpiece shape and t is thickness of the workpiece. Figure 7 illustrates the difference between desired and deformed geometry after springback. Design constraints are imposed to limit the amount of effective plastic strain that may result in material failure or severe necking. The minimum thickness of the each section is also limited. Limits on u_i are established according to workpiece geometry and kinematics. Because u_i represent the structure's relative movements, the initial values are set at zero.

The design optimization problem is solved using the sequential quadratic programming method in DOT[22] by supplying mesh-free analysis results and design sensitivity information. At each iteration, the initial geometry of the problem is updated.

The design optimization problem is converged in four iterations, which is quite fast considering the degree of nonlinearity involved in the structural analysis. Figure 8a provides a history for cost function G during optimization. The cost function, which is the difference between a desired shape and the deformed shape after springback, is reduced by up to 24% of the initial design. All constraints are satisfied with no active constraint at the optimal design. Figure 8b shows the design parameter history. The corner radius u_4 of the rigid die is significantly increased to reduce overdeflection of the workpiece at the binder part. The corner radius u_3 of the punch is decreased so that the workpiece remains vertical. Note that the binder force, which is controlled by u_6, is decreased from the initial design, which in turn reduces the frictional force.

The deformed shapes of the initial and optimal designs are shown in Fig. 9. Overdeflection of the initial design around the blank holder area is significantly reduced to match the desired shape shown in Fig. 7. The vertical slope is also improved as compared to the initial design. However, it turns out that making a 90-deg vertical slope is very difficult based on current manufacturing processes unless a springforward method is used, which is not possible for this particular deepdrawing process. Note that the radius of the bottom corner is increased in the optimum design. Nevertheless, an effort to compensate for this region will result in a larger deviation from the desired shape in other regions.

Figure 10 compares the effective plastic strain distributions for initial (Fig. 10a) and optimal (Fig. 10b) designs. The maximum level of effective plastic strain at the optimum design point is 12%

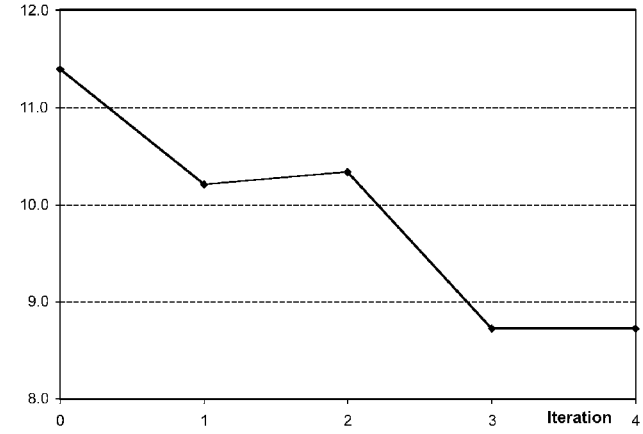

a) Cost function history

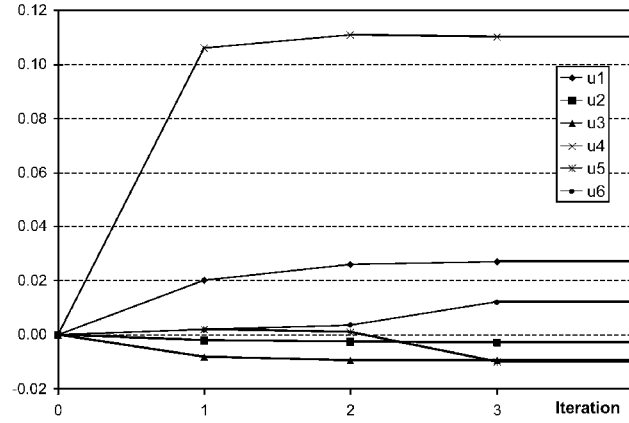

b) Design parameter history

Fig. 8 Deepdrawing optimization history.

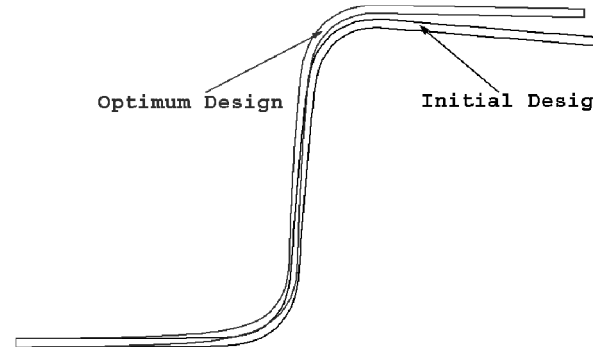

Fig. 9 Final deformed shapes of initial and optimum designs after springback.

less than that of the initial design. The amount of springback is also reduced.

In the deepdrawing process, a necking amount proportonal to the plastic deformation is an important criterion in determining the quality of the product. In this paper, the necking amount is measured according to the change of thickness of the blank. Figure 11 shows thickness reductions for the initial and optimal designs. It is clear that the optimum design shows less plastic deformation compared to the initial design, which is consistent with the effective plastic strain distribution in Fig. 10. Because the plastic deformation is volume conserving, the area of the graph is transformed into an increase of the blank's cord length. The area of initial design in Fig. 11 is 1.18 mm^2, whereas it is 0.716 mm^2 for the optimal design.

An initial cord length of 75 mm is stretched during simulation to 76.46 mm, whereas the total cord length is 75.87 mm in the optimal design, which is consistent with a reduction of plastic deformation in the optimum design. Figure 11 provides parallel results using a change of cord lengths for initial and optimal design models.

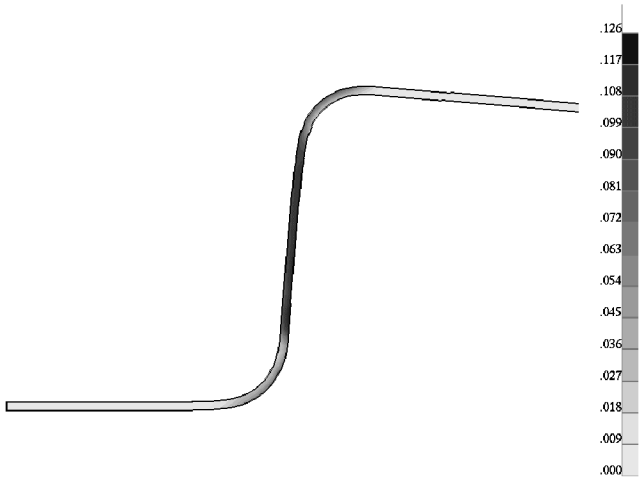

a) Initial design

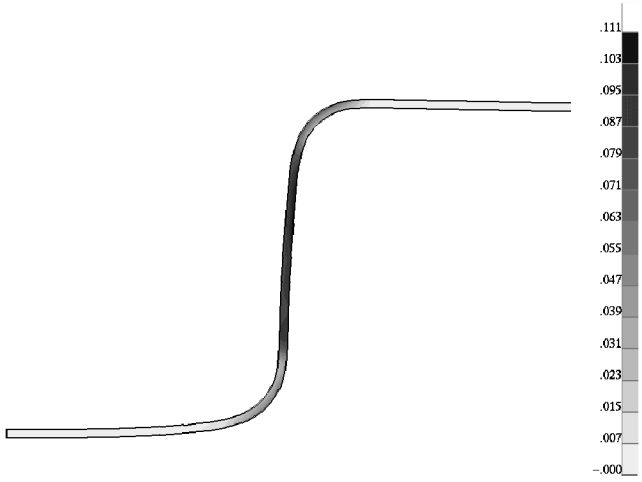

b) Optimum design

Fig. 10 Effective plastic strain distributions.

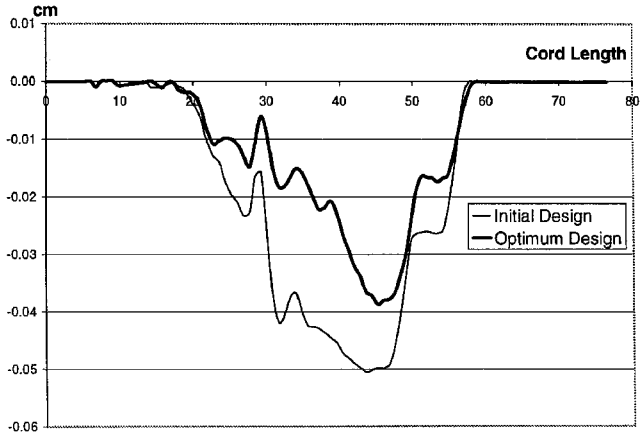

Fig. 11 Thickness reduction of workpiece.

V. Conclusions

Very efficient and accurate methods of numerical simulation and DSA methods are proposed for a deepdrawing process design. These methods rely on a mesh-free nonlinear analysis and continuum-based DSA. The rigid-body shape and the workpiece thickness are considered for design parameters. The optimal design results show the feasibility of the proposed method for a deepdrawing process.

Acknowledgments

This research is supported by General Motors and the National Science Foundation/Defense Advanced Research Projects Agency. The support is gratefully acknowledged.

References

[1]Antunez, H. J., and Kleiber, M., "Sensitivity of Forming Processes to Shape Parameters," *Computer Methods in Applied Mechanics and Engineering*, Vol. 137, Nos. 3–4, 1996, pp. 189–206.

[2]Maniatty, A. M., and Chen, M. F., "Shape Sensitivity Analysis for Steady Metal-Forming Processes," *International Journal for Numerical Methods in Engineering*, Vol. 39, No. 7, 1996, pp. 1199–1217.

[3]Zhao, G. Q., Wright, E., and Grandhi, R. V., "Preform Die Shape Design in Metal Forming Using an Optimization Method," *International Journal for Numerical Methods in Engineering*, Vol. 40, No. 7, 1997, pp. 1213–1230.

[4]Chung, S. H., and Hwang, S. M., "Optimal Process Design in Non-Isothermal, Non-Steady Metal Forming by the Finite Element Method," *International Journal for Numerical Methods in Engineering*, Vol. 42, No. 8, 1998, pp. 1343–1390.

[5]Balagangadhar, D., and Tortorelli, D. A., "Design and Analysis of Large Deformation Continuous Elastoplastic Manufacturing Processes via a Steady Displacement-Based Formulation," *Proceedings of the 7th AIAA/USAF/NASA/ ISSMO Symposium on Multidisciplinary Analysis and Optimization*, AIAA, Reston, VA, 1998, pp. 1396–1406.

[6]Badrinarayanan, S., and Zabaras, N., "A Sensitivity Analysis for the Optimal Design of Metal-Forming Processes," *Computer Methods in Applied Mechanics and Engineering*, Vol. 129, No. 4, 1996, pp. 319–348.

[7]Wiechmann, W., and Barthold, F. J., "Remarks on Variational Design Sensitivity Analysis of Structures with Large Elastoplastic Deformations," *Proceedings of the 7th AIAA/USAF/ NASA/ISSMO Symposium on Multidisciplinary Analysis and Optimization*, AIAA, Reston, VA, 1998, pp. 349–358.

[8]Guo, Y. Q., Batoz, J. L., Naceur, H., Bouabdallah, S., Mercier, F., and Barlet, O., "Recent Developments on the Analysis and Optimum Design of Sheet Metal Forming Parts Using a Simplified Inverse Approach," *Computers and Structures*, Vol. 78, Nos. 1–3, 2000, pp. 133–148.

[9]Karafillis, A. P., and Boyce, M. C., "Tooling and Binder Design for Sheet Metal Forming Process Compensating Springback Error," *International Journal of Machine Tools and Manufacture*, Vol. 36, No. 4, 1996, pp. 503–526.

[10]Kim, N. H., Choi, K. K., and Chen, J. S., "Structural Optimization of Finite Deformation Elastoplasticity Using Continuum-Based Design Sensitivity Formulation," *Computers and Structures*, Vol. 79, No. 20–21, 2001, pp. 1385–1405.

[11]Kim, N. H., Choi, K. K., and Chen, J. S., "Shape Design Sensitivity Analysis and Optimization of Elastoplasticity with Frictional Contact," *AIAA Journal*, Vol. 38, No. 9, 2000, pp. 1742–1753.

[12]Liu, W. K., Jun, S., and Zhang, Y. F., "Reproducing Kernel Particle Methods," *International Journal for Numerical Methods in Fluids*," Vol. 20, Nos. 8–9, 1995, pp. 1081–1106.

[13]Chen, J. S., Pan, C., Roque, C. M. D. L., and Wang, H. P., "A Lagrangian Reproducing Kernel Particle Method for Metal Forming Analysis," *Computational Mechanics*, Vol. 22, No. 3, 1998, pp. 289–307.

[14]Simo, J. C., and Pister, K. S., "Remarks on Rate Constitutive Equations for Finite Deformation Problem: Computational Implications," *Computer Methods in Applied Mechanics and Engineering*, Vol. 46, No. 2, 1984, pp. 201–215.

[15]Lee, E. H., "Elastic–Plastic Deformation at Finite Strains," *Journal of Applied Mechanics*, Vol. 36, No. 1, 1969, pp. 1–6.

[16]Simo, J. C., "Algorithms for Static and Dynamic Multiplicative Plasticity that Preserve the Classical Return Mapping Schemes of the Infinitesimal Theory," *Computer Methods in Applied Mechanics and Engineering*, Vol. 99, No. 1, 1992, pp. 61–112.

[17]Chen, J. S., Wu, C. T., Yoon, S., and You, Y., "Stabilized Conforming Nodal Integration for Galerkin Meshfree Methods," *International Journal for Numerical Methods in Engineering*, Vol. 50, No. 2, 2001, pp. 435–466.

[18]Chen, J. S., and Wang, H. P., "New Boundary Condition Treatments for Meshless Computation of Contact Problems," *Computer Methods in Applied Mechanics and Engineering*, Vol. 187, Nos. 3–4, 2000, pp. 441–468

[19]Haug, E. J., Choi, K. K., and Komkov, V., *Design Sensitivity Analysis of Structural Systems*, Academic Press, New York, 1986, pp. 32–34.

[20]*MSC/PATRAN User's Manual*, MacNeal–Swendler Corp., Los Angeles, 1999.

[21]Choi, K. K., and Chang, K. H., "A Study of Design Velocity Field Computation for Shape Optimal Design," *Finite Elements in Analysis and Design*, Vol. 15, No. 4, 1994, pp. 317–341.

[22]Vanderplaats, G. N., *DOT User's Manual*, VMA Corp., Colorado Springs, CO, 1997, pp. 167–169.

S. Saigal
Associate Editor